Research Paper

Intravitreal injection of anti-miRs against miR-142-3p reduces angiogenesis and microglia activation in a mouse model of laser-induced choroidal neovascularization

Quentin Roblain[1,2], Thomas Louis[1], Cassandre Yip[1], Louis Baudin[1], Ingrid Struman[3], Vincenza Caolo[5], Vincent Lambert[1,4], Julie Lecomte[1,*], Agnès Noël[1,*], Stephane Heymans[2,5,*]

[1]Laboratory of Tumor and Development Biology, GIGA-Cancer, University of Liège, Liège, Belgium
[2]Department of Cardiology, CARIM School for Cardiovascular Diseases, Faculty of Health, Medicine and Life Sciences, Maastricht University, Maastricht, The Netherlands
[3]Molecular Angiogenesis Laboratory, GIGA-Cancer, University of Liège, Liège, Belgium
[4]Ophthalmic Tissue Bank, Department of Ophthalmology, University Hospital of Liège, Sart-Tilman, Belgium
[5]Department of Cardiovascular Sciences, Centre for Molecular and Vascular Biology, KU Leuven, Leuven, Belgium
*Equal contribution

Correspondence to: Agnès Noël; email: Agnes.Noel@uliege.be

ABSTRACT

Age-related macular degeneration (AMD) is a worldwide leading cause of blindness affecting individuals over 50 years old. The most aggressive form, wet AMD, is characterized by choroidal neovascularization (CNV) and inflammation involving microglia recruitment. By using a laser-induced CNV mouse model, we provide evidence for a key role played by miR-142-3p during CNV formation. MiR-142-3p was overexpressed in murine CNV lesions and its pharmacological inhibition decreased vascular and microglia densities by 46% and 30%, respectively. Consistently, miR-142-3p overexpression with mimics resulted in an increase of 136% and 126% of blood vessels and microglia recruitment. Interestingly, miR-142-3p expression was linked to the activation state of mouse microglia cells as determined by morphological analysis (cell solidity) through a computational method. In vitro, miR-142-3p overexpression in human microglia cells (HMC3) modulated microglia activation, as shown by CD68 levels. Interestingly, miR142-3p modulation also regulated the production of VEGF-A, the main pro-angiogenic factor. Together, these data strongly support the unprecedented importance of miR-142-3p-dependent vascular-inflammation axis during CNV progression, through microglia activation.

INTRODUCTION

Globally, 2.2 billion people suffer of vision impairment or blindness [1]. Age-related macular degeneration (AMD) is the fourth leading cause of blindness worldwide [2], affecting 8.7 % of population. This percentage is expected to increase due to the ageing population [3]. Although less frequent than atrophic (or dry) AMD, neovascular (or wet) AMD represents the most vision-threatening form of the disease [4]. It is mainly characterized by choroidal neovascularization (CNV), the formation of abnormal blood vessels arising from the choroid and invading the subretinal space, leading to vision impairment [5]. This angiogenic process is associated with the recruitment and proliferation of inflammatory cells including neutrophils, macrophages and microglia [6, 7]. The latter cells are the main resident immune cells and contributors to the innate immunity within the central nervous system, including the retina. At the

experimental level, rodent models of laser-induced CNV are the most broadly used for neovascular AMD pre-clinical research [7, 8]. They recapitulate the angiogenic and inflammatory phases of the disease including microglia implication. Antibody-based anti-VEGF (Vascular Endothelium Growth Factor) therapy is still the golden standard for the management of neovascular AMD [9]. Unfortunately, around one fifth of neovascular AMD patients do not or poorly respond to anti-VEGF therapy [10]. Therefore, additional therapies are urgently required.

MicroRNAs, also called miRs or miRNAs, are short non-coding RNA species of about 20-24 nucleotides length, which act as post-transcriptional gene-expression regulators. A single mature microRNA can bind to several mRNAs and a single mRNA can be targeted by several miRNAs [11–13]. Many ocular diseases are regulated by short non-coding RNAs, and a growing body of literature related to miRNA complications in eye disorders is currently emerging [14, 15]. To date, several teams have focused on establishing microRNAs as potential AMD biomarkers in both human and mouse study [16, 17]. However, only a few of these studies addressed the question of a functional role of microRNAs in AMD [18]. Through their capacity to regulate biological processes such as angiogenesis and inflammation [19, 20], a functional contribution of miRNA in AMD is expected, but poorly documented. Hence, miRNA as therapeutic target for the treatment of AMD is an emerging concept for future drug design.

In the present study, we searched for microRNAs with functional implication in CNV development. We first determined the expression profile of a set of angiogenesis and inflammation-related microRNAs in mouse CNV lesions. Inhibition and overexpression of miR-142-3p, one of the top dysregulated microRNAs, regulated both vascular and inflammatory phenotypes. Notably, microglia recruitment and activation were enhanced by miR-142-3p mimic and reduced by miR-142-3p inhibitor both *in vitro* and *in vivo*. Our work provides evidence that miR-142-3p is a functional mediator during CNV progression and acts as a microglia cell activator. MiR-142-3p is worth considering as a target for future neovascular AMD therapeutics.

RESULTS

miR-142-3p is overexpressed in a laser-induced CNV mouse model

Laser microdissection was used to isolate three types of samples from mice subjected or not to laser-induced CNV: i) control choroid from control mice (not subjected to CNV induction), ii) CNV lesions, and iii) adjacent choroid (healthy choroid adjacent to CNV lesion) (Figure 1A). In a pilot experiment, the expression profile of 15 angiogenesis and/or inflammation-related microRNAs were determined 7 days post-induction by qRT-PCR in the 3 regions of interest (Figure 1B). Although probably not extensive enough, we focused our attention only on these 15 microRNAs i) because of limited RNA availability after laser microdissection and ii) because these microRNAs are reported angiogenesis and/or inflammation mediators. Among those microRNAs tested, only 4 were dysregulated: miR-21-5p, miR-34a-5p and miR-142-3p increased whereas miR-574-3p decreased upon laser-induction. To further confirm the overexpression of miR-142-3p in laser-induced CNV mouse, laser microdissection was repeated 7 days as well as 5 days post laser-induction. Interestingly, the miR-142-3p increased in the CNV lesions, both at days 5 and 7 post laser induction (Figure 1C), and correlated with the overexpression of uPA (urokinase plasminogen activator) used here as a CNV-disease marker [21] (Figure 1D and Supplementary Figure 1). Taken together, these data suggest that miR-142-3p could be of CNV progression in the laser-induced CNV mouse model.

Modulation of miR-142-3p expression alters neovascularization and inflammation in CNV mouse model

Intravitreal injections of miR-142-3p inhibitor or mimic allowed us to evaluate the functional role of miR-142-3p during CNV progression in the laser-induced CNV mouse model. CNV lesion thickness, as assessed by OCT measurements, was lower in mice injected with miR-142-3p inhibitor when compared to control inhibitor (Figure 2A) (p = 0.0149). This inhibitor reduced by 46 % the blood vessel density in CNV mouse (Figure 2B, top panels) (p = 0.0157). Concomitantly, microglia area, a major component of the innate immunity in the eye, was decreased by 30 % upon miR-142-3p inhibition (Figure 2B, bottom panels) (p = 0.0292). Therefore, miR-142-3p inhibition alleviates CNV progression by decreasing neo-vascularization and inflammation. Inversely, the overexpression of miR-142-3p through mimic injection slightly enhanced CNV lesion thickness (Figure 3A) (p = 0.407). It also increased the angiogenic response by 136 % (Figure 3B, top panels) (p = 0.0233) and microglia cell recruitment by 126 % (Figure 3B, bottom panels) (p = 0.0441). For both inhibitor and mimic conditions, miR-142-3p retinal levels were measured to assess its inhibition/overexpression (Supplementary Figures 2, 3). Altogether, the
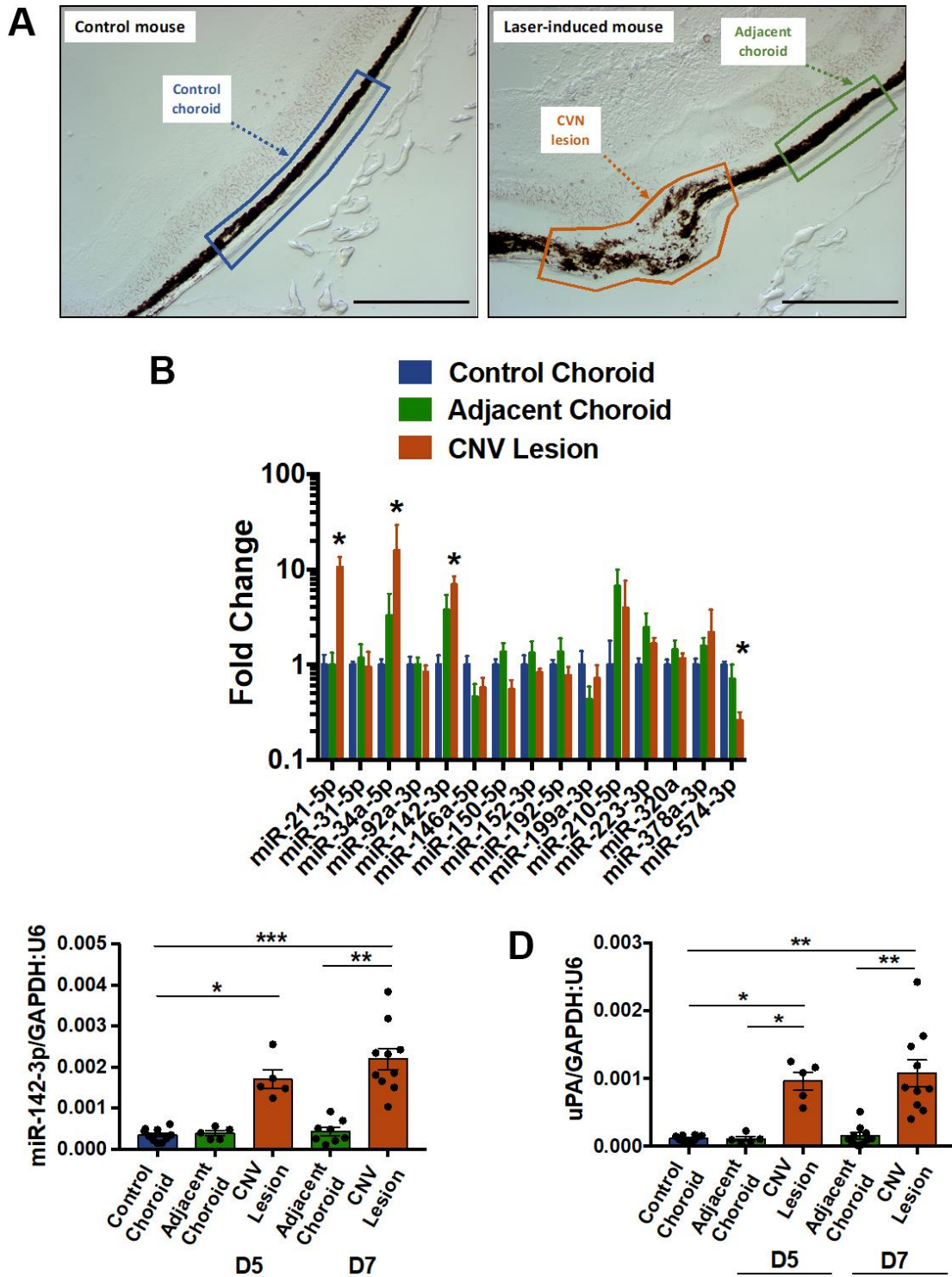
Figure 1. MiR-142-3p is overexpressed in a laser-induced CNV mouse model. (**A**) Cryosections of control mouse (untreated) and laser-induced mouse delineating the different regions of interest (ROI). These ROIs, namely control choroid (in blue), adjacent choroid (in green) and CNV lesion (in orange), were isolated by laser microdissection. Scale bar = 250 μm. (**B**) MicroRNA expression in CNV lesion and adjacent choroid compared to control choroid, 7 days after laser induction. Results of CNV lesion and adjacent choroid are expressed as fold change to control choroid. Results are presented as mean +- SEM. One-way ANOVA followed by multiple comparisons test (n = 5 per experimental group). (**C, D**) Overexpression of miR-142-3p (C), and uPA (D), a CNV-disease marker, at day 5 (D5) and day 7 (D7). MiR-142-3p and uPA are specifically overexpressed in CNV lesion 5 and 7 days post laser induction. qRT-PCR results are presented as mean +- SEM. One-way ANOVA + multiple comparisons test (n = 10 for control choroid, n = 5 for adjacent choroid and CNV lesion D5, n = 10 for adjacent choroid and CNV lesion D7) (* = p ≤ 0.05; ** = p ≤ 0.01; *** = p ≤ 0.001).
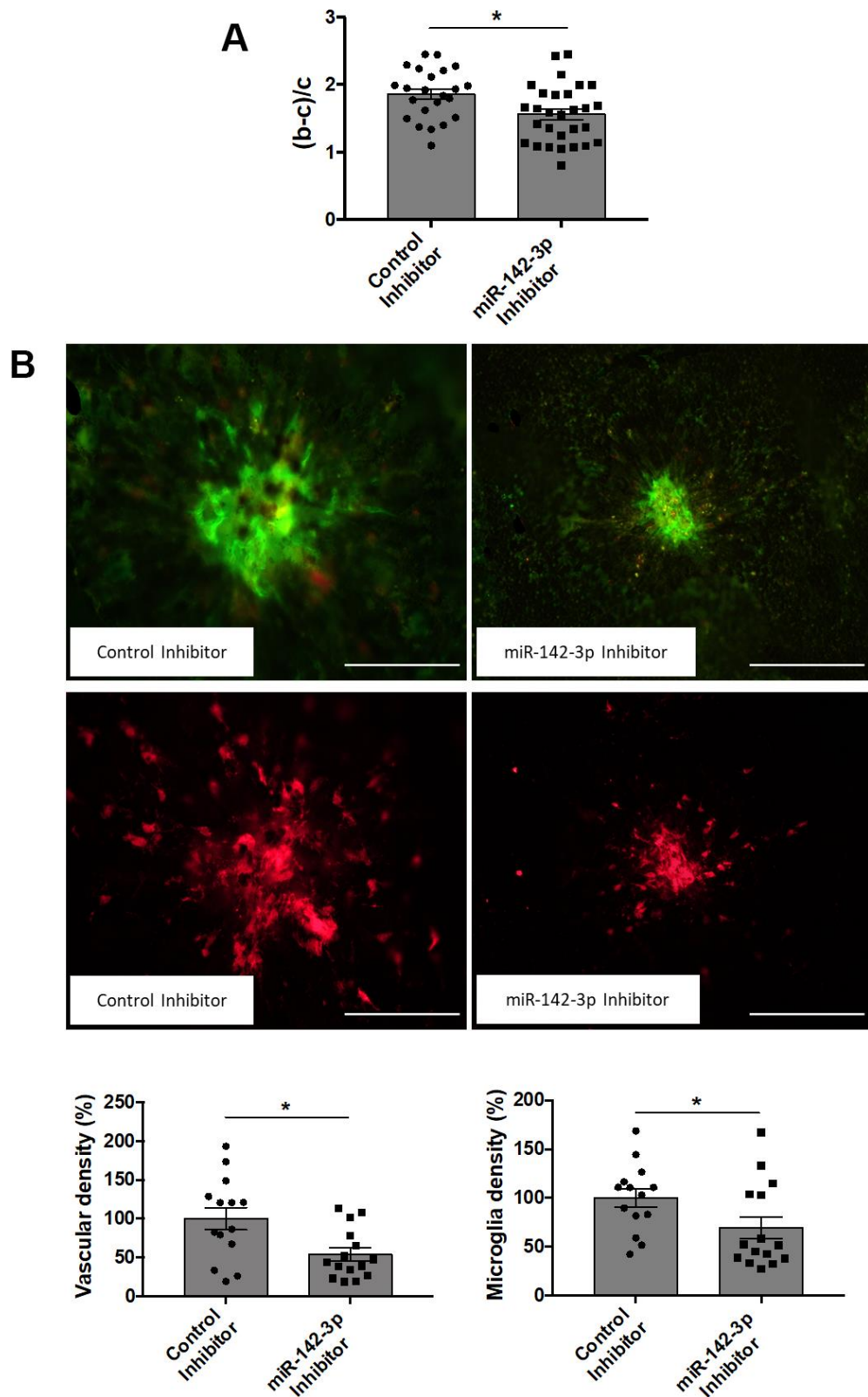
Figure 2. Inhibition of miR-142-3p in a laser-induced CNV mouse model decreases both vascular and inflammatory phenotypes. (**A**) OCT measurement presented as (b-c)/c ratios where b is the CNV lesion thickness and c is the adjacent choroid thickness. b and c were measured just prior to sacrifice (n = 23-29 per experimental group). (**B**) Flat-mounted choroids showing vascular (in green) and microglia (in red) density and corresponding quantification. Scale bar = 250 μm (n = 14-15 per experimental group). All results are presented as mean +- SEM. Mann Whitney test (* = p ≤ 0.05).
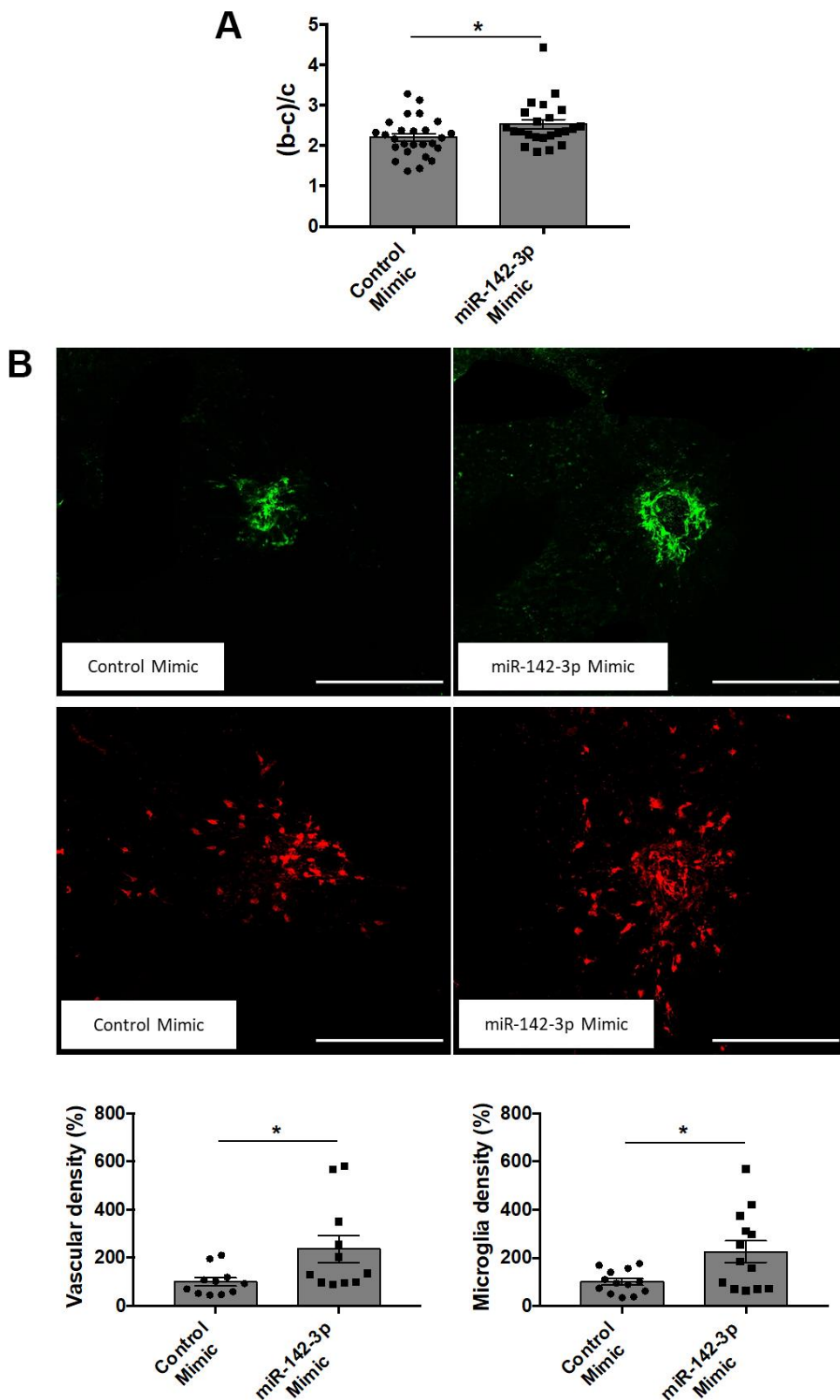
Figure 3. Overexpression of miR-142-3p in a laser-induced CNV mouse model increases both vascular and inflammatory phenotypes. (**A**) OCT measurement presented as (b-c)/c ratios where b is the CNV lesion thickness and c is the adjacent choroid thickness. b and c were measured just prior to sacrifice (n = 24-26 per experimental group). (**B**) Flat-mounted choroids showing vascular (in green) and microglia (in red) density and corresponding quantification. Scale bar = 250 μm (n = 11-13 per experimental group). All results are presented as mean +- SEM. Mann Whitney test (* = p ≤ 0.05).

modulation of miR-142-3p expression in CNV mouse model revealed a functional role of this microRNA during CNV progression. Intriguingly, both the vascular and microglia components of CNV lesions were affected by miR-142-3p modulation.

Retina microglia cell activation is closely linked to miR-142-3p expression

Microglia cells are resident immune cells of the central nervous system, including the retina. In laser-induced mouse model of CNV, microglia are recruited from the retina and invade the underlying CNV lesion [22, 23]. Under activation in inflammatory conditions, resting microglia cells lose their highly ramified morphology and gain an amoeboid shape. To assess the effect of miR-142-3p on retina microglia cell shape *in vivo*, an innovative computerized quantification method has been set up. Cell solidity corresponds to the ratio between the cell volume and its convex volume, and reflects microglia activation (Figure 4A). While activated amoeboid microglia cells are characterized by a solidity closer to 1 (which characterizes a round cell), resting ramified microglia cells are characterized by a solidity closer to 0 (Figure 4A). Each portion of the whole retina corresponding to a CNV lesion and its surrounding tissue was imaged at the 20X magnification to insure an optimal resolution for cell solidity analysis (Figure 4B). Raw images were processed and binarized for computerized quantification, which allowed a clear discrimination of every single microglia cell within the entire image (Figure 4C and Supplementary Figure 4). Interestingly, this computerized image analysis revealed that miR-142-3p inhibitor and miR-142-3p mimic impacted drastically the morphology of retina microglia cell (Figure 4D and Supplementary Figure 5). While miR-142-3p inhibitor decreased microglia solidity and thus microglia activation, miR-142-3p mimic had the opposite effect. Altogether, these data suggest that miR-142-3p contributes *in vivo* to microglia cell activation.

miR-142-3p regulates the activation of human microglia cells under pro-inflammatory conditions

Transfection of human microglia HMC3 cells with miR-142-3p mimic drastically increased miR-142-3p expression (Figure 5A, right panel). It also decreased the production of its previously described target, BCLAF1, both at mRNA (Figure 5B, right panel) and protein (Figure 5C) levels [24]. BCLAF1 was used here to validate the efficacy of miR-142-3p mimic. Alongside with its effect on BCLAF1 expression, miR-142-3p overexpression also influenced HMC3 activation state as assessed by increased CD68 level (Figure 5D, right panel), a marker of microglia

activation [25, 26]. Interestingly, VEGF-A transcript level (Figure 5E, right panel) increased upon miR-142-3p mimic, which could contribute to the effect observed *in vivo* on the angiogenic response. When using the inhibitor, only a slight decrease of miR-142-3p expression was observed (Figure 5A, left panel) without any effect on BCLAF1, CD68 and VEGF-A levels (Figure 5B–5E, left panels). Such a low effect of the inhibitor may be related to the low basal level of miR-142-3p in HMC3 cell line.

Our data *in vitro* confirm the *in vivo* findings of the biological implication of miR-142-3p in microglia activation. This is further supported by the concomitant increase of miR-142-3p and CD68 expressions in HMC3 cells stimulated by IFNγ or LPS (Figure 5F). Taken together, these data revealed a strong link between the activation state of microglia cell and miR-142-3p expression.

DISCUSSION

The present study unveils a functional role of miR-142-3p in stimulating CNV formation in a mouse model of wet AMD. This novel concept is supported by i) the overexpression of miR-142-3p in CNV lesions, and by ii) the impact of this miRNA modulation (inhibition/overexpression) on both vascular and inflammatory phenotypes. While inhibition of miR-142-3p caused a subsequent decrease of angiogenesis, its overexpression had the opposite effect. Beside its effect on angiogenesis, administration of miR-142-3p activates microglia cells -part of the inflammatory process- both *in vivo* and *in vitro*. Our data provide evidence for a pivotal role played by miR-142-3p during CNV progression and particularly on microglia activation.

The originality of our approach relies on the laser microdissection, which enables us to isolate CNV tissue devoid of any surrounding healthy tissue that could have biased the microRNA profile [27]. Indeed, previous studies in CNV mouse primarily investigated microRNAs circulating in the blood [17, 28] or present in the entire RPE-choroid-sclera complexes [29]. It is noteworthy that CNV lesion sites only englobe 2.5% of total choroid tissue, making entire choroid complexes highly heterogenous mixes of healthy and non-healthy tissue. Among the microRNAs tested, 4 were dysregulated: miR-21-5p, miR-34a-5p and miR-142-3p increased, whereas miR-574-3p decreased upon laser-induction. In line with our data, miR-21-5p was previously reported as strongly up-regulated in RPE-choroid-sclera complex [29]. MiR-21-5p is a well-known pro-angiogenic microRNA in different pathologies [30, 31] and is highly abundant in human retinal endothelial cells [32]. Concomitantly to the
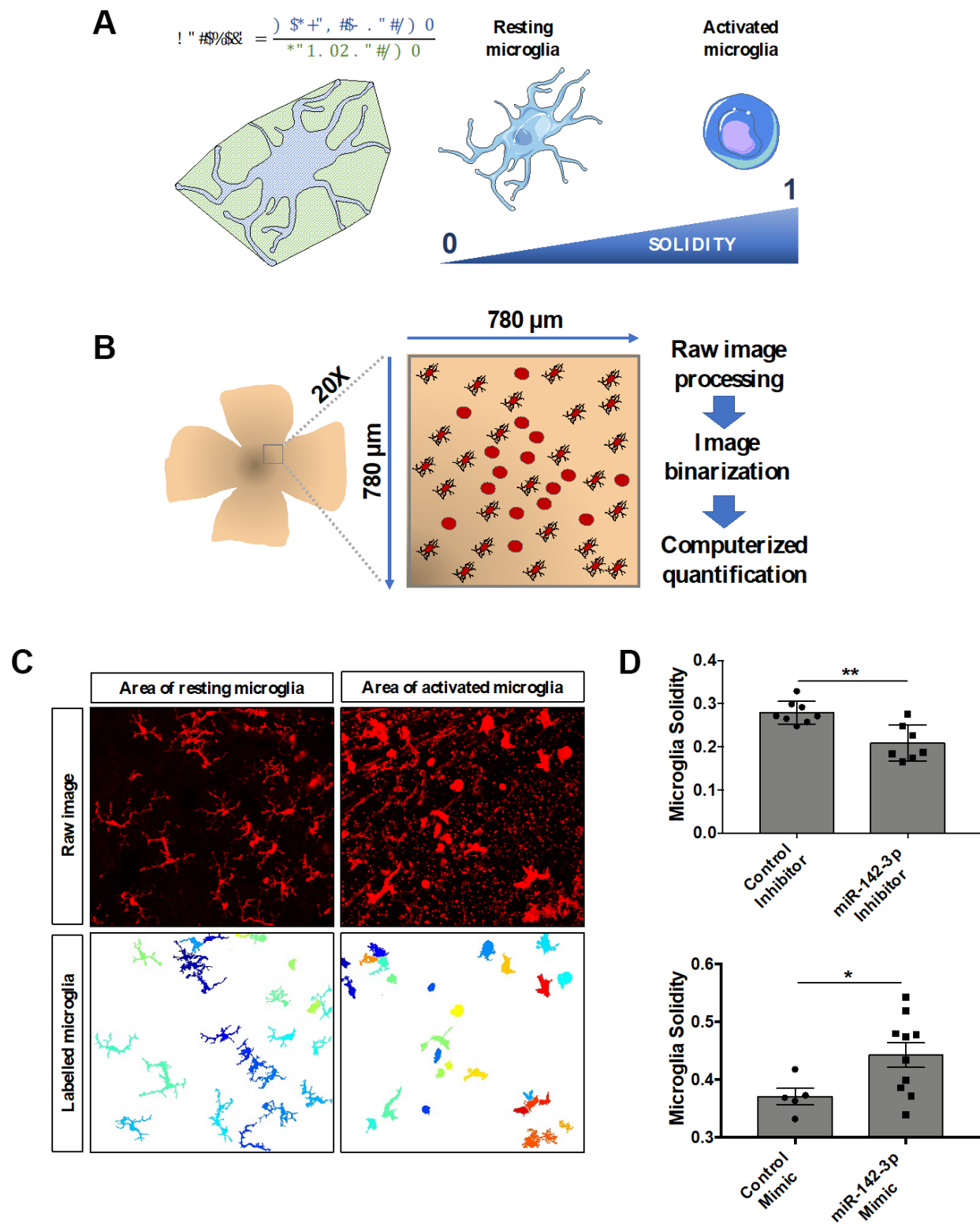
Figure 4. MiR-142-3p influences microglia cell activation state *in vivo*. (**A**) Characterization of microglia morphology via cell solidity. The solidity of an object is defined as the ratio between its volume and its convex volume. Resting microglia are highly ramified while activated microglia present an amoeboid shape, with no or small ramifications. Activated microglia are characterized by a higher solidity. (**B**) CNV lesion area of flat-mounted retinas and surrounding healthy tissue were imaged at the 20X magnification and then processed and quantified. (**C**) Representative raw images and corresponding labelled images of resting and activated microglia area. (**D**) Microglia activity measured around the CNV lesion in mice injected with either miR-142-3p inhibitor or mimic and relative controls (n = 5-10 per experimental group). All results are presented as mean +- SEM. Mann Whitney test (* = p ≤ 0.05; ** = p ≤ 0.01).
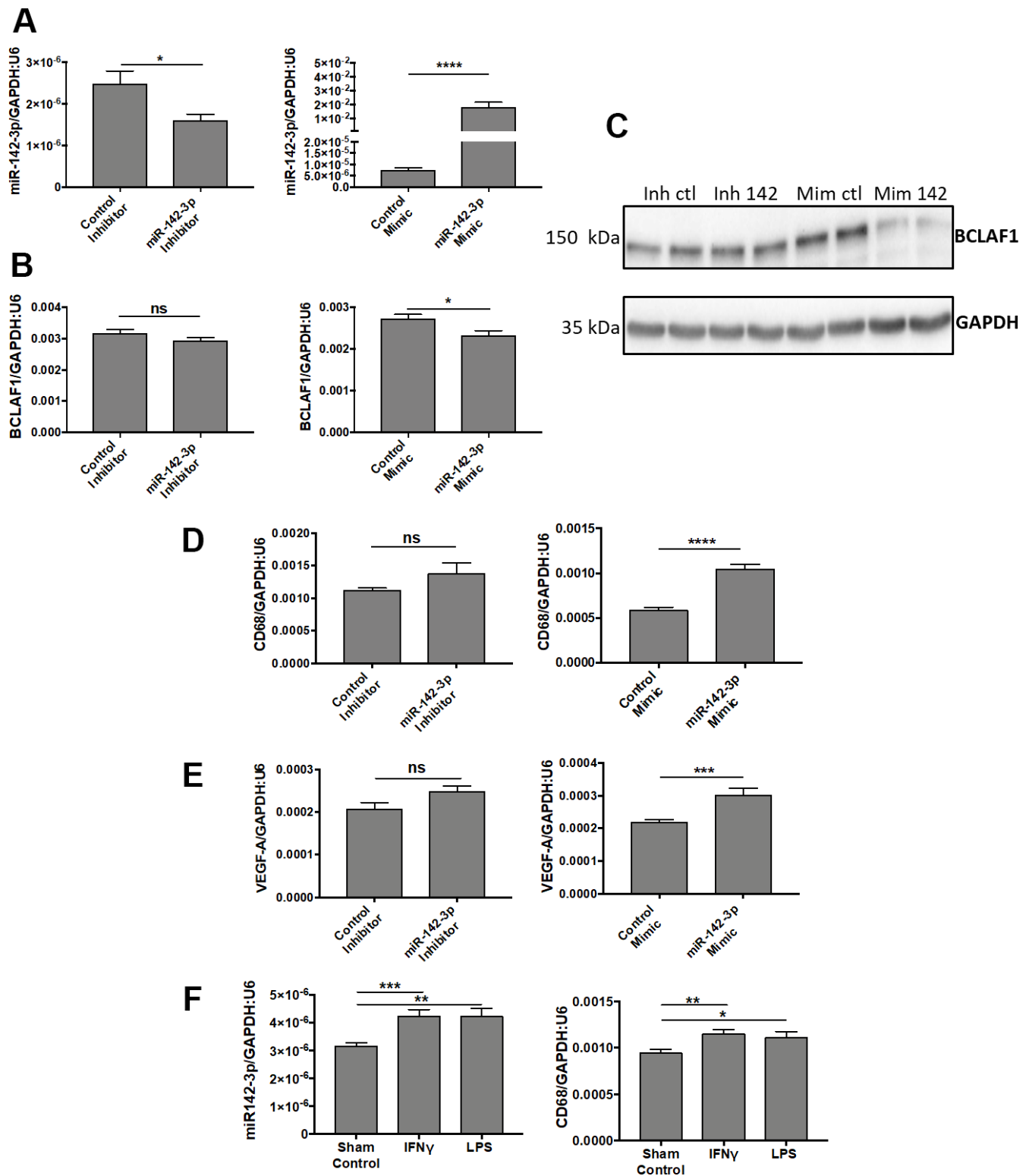
Figure 5. MiR-142-3p regulates the activation of human microglia cells under pro-inflammatory conditions. (**A–C**) Transfections of miR-142-3p inhibitor and mimic lead to decreased and increased miR-142-3p level, respectively (**A**). Transfection of miR-142-3p mimic decreased BCLAF1 levels, a previously identified target of miR-142-3p, both at the transcript level (**B**) and protein level (**C**). (**D, E**) Effects on CD68 level (**D**) or VEGF-A (**E**) in HMC3 transfected with miR-142-3p inhibitor or mimic and relative controls. Only miR-142-3p mimic was able to induce CD68 et VEGF-A production. (**F**) HMC3 stimulated with either IFN$^\gamma$ or LPS for 24 hours overexpress miR-142-3p as long with CD68. All qRT-PCR results are presented as mean +- SEM. Mann Whitney test. (* = p ≤ 0.05; ** = p ≤ 0.01; *** = p ≤ 0.001; **** = p ≤ 0.0001; ns = not significant).

overexpression of miR-34a-5p in our samples, this microRNA was found to be upregulated in serum of AMD patients [33] and in hydrogen peroxide-induced prematurely senescent ARPE-19 cells [34], possibly leading thus to AMD progression. Concerning miR-574-3p, its downregulation in the CNV model did not prompt us to consider it for an inhibition strategy.

Here, we identified miR-142-3p as a specific CNV lesion microRNA, being upregulated both 5- and 7-days post laser-induction and displaying a correlation with uPA, a well-established CNV disease marker [21]. MiR-142 gene is a broadly conserved miRNA gene among species that gives rise to two distinct mature forms, miR-142-3p and miR-142-5p. MiR-142 is involved in stem cell fate, cardiomyocyte hypertrophy, cancer, immune tolerance and hematopoiesis, as previously reviewed [35]. Both vascular [24] and inflammatory [36] functions have been attributed to this microRNA. Interestingly, miR-142-3p expression is upregulated in a mouse model of retinal degeneration [37], but its biological role in ocular disease, including wet AMD, remained unknown. The increase of miR-142-3p in CNV goes in parallel with macrophage recruitment, as well as the increase in vascular density [7]. Thus, miR-142-3p expression was associated with two interconnected hallmarks of the disease, namely inflammation and angiogenesis. Interestingly, miR-142-5p, the other mature strand of miR-142, was not detected in our laser-induced CNV mouse model. This lack of expression may reinforce the specific function of miR-142-3p only, and not miR-142-5p, during CNV progression. Previous studies revealed that the cellular source of miR-142-3p may be more immune-related rather than vascular-related [38–40]. Accordingly, miR-142-3p expression in human microglia cells increased upon IFNγ or LPS stimulation, and correlated with CD68 level, a marker of activated microglia. To evaluate the functional role of miR-142-3p during CNV, miR-142-3p inhibitor or mimic were injected into the vitreous chamber of CNV mouse. Intravitreal injections are routinely used by clinicians to deliver anti-VEGF drugs to wet AMD patients [41]. On one hand, intravitreal injection of miR-142-3p inhibitor decreased the vascular density in flat-mounted choroids, while injection of miR-142-3p mimic conversely increased it. Those findings were further confirmed by alterations of CNV lesion thickness measured via OCT. Furthermore, intravitreal miR-142-3p inhibition alleviated microglia density, while miR-142-3p mimic increased it. The biodistribution of miR-142-3p inhibitor/mimic within mouse eyeball after intravitreal injections is not known. Still, we noticed an impact on both retinal and choroidal tissues, suggesting a wide diffusion of the molecule. Before using this kind of inhibitor in the clinic, a better understanding of its diffusion within the eye and a

target cell optimization would be needed. These improvements may imply less frequent injections than current therapy.

Microglia are the immune resident cells of the central nervous system, constantly screening their environment for pathogens and ready to migrate, proliferate and phagocyte if needed. In physiological conditions, retinal microglia cells exhibit a highly ramified morphology, shifting to a more amoeboid shape under activation [23]. In the laser-induced CNV context, microglia are known to migrate from retina and invade CNV lesion site, starting 4-days post laser-induction [22]. Various cellular morphology parameters exist to describe microglia shape [42, 43], but cell solidity has been described as the most appropriate one for assessing the amoeboid shape of activated microglia, and thus microglia activation [44]. An innovative computerized imaging and quantification technique revealed that miR-142-3p inhibition/overexpression decreases/increases retinal microglia cell solidity *in vivo*, in line with our *in vitro* data of miR-142-3p mediated microglia activation. Our data suggest that miR-142-3p stimulates the activation of microglia in the retina and their migration to the CNV lesion site, located within the choroid. Accordingly, miR-142-3p is one of the top up-regulated microRNA in primary microglia isolated from rat pup's brain under LPS stimulation [45]. Besides morphological analysis, future studies may evaluate mouse microglia activation state through transcriptomic and surface marker analyses. Interestingly, in human microglia culture, miR-142-3p mimic enhanced drastically miR-142-3p levels, as well as CD68 expression, a marker of activated microglia [25, 26]. An interesting finding is the concomitant up-regulation of VEGF-A, a key molecular mediator of CNV progression [46]. This demonstrates that miR-142-3p is able to modulate both inflammatory and vascular responses, two intimately linked processes associated to CNV progression [47]. Interestingly, CD68 was also upregulated in HMC3 stimulated by IFNγ or LPS, leading to a pro-inflammatory state [48, 49]. This observation supports the concept that miR-142-3p is a mediator of inflammation triggering microglia cell activation and is in line with our *in vivo* data. How miR-142-3p modulates CD68 and VEGF-A production remains to be elucidated. However, our data support the concept that miR-142-3p could be a new intermediate in the vascular-inflammatory axis during CNV progression, through microglia activation.

In conclusion, miR-142-3p may exacerbate CNV by enhancing microglia migration and activation, and

therefore is worth considering as a potential therapeutic target in AMD.

MATERIALS AND METHODS

Laser-induced choroidal neovascularization mouse model

CNV was induced in mice by laser-mediated choroid burn as previously described [7]. Briefly, 6 to 8 weeks old C57Bl6 mice (all males) (Janvier, France) were anesthetized by intraperitoneal injection of a mixture of ketamine (50 mg/kg) and medetomidine (0.5 mg/kg). A few minutes before laser induction, pupils were dilated with Tropicol (Théa Pharma, France). Four laser burns per eye were performed with MicronIV instrument (Phoenix Lab, USA) leading to Bruch's membrane local destruction and the subsequent choroidal neovascularization. Mice were than woken up by intraperitoneal administration of atipamezole (1mg/kg). Mice were sacrificed 5 (D5) or 7 days (D7) after laser induction by cervical dislocation. All *in vivo* experiments were approved by the local Animal Ethic Commission (File number 17-1986, "Commission d'éthique de l'utilisation des animaux de l'Université de Liège").

Laser microdissection of the choroid

Mice subjected or not to CNV induction were sacrificed at D5 or D7 post-laser burn (n = 5-10 per experimental group, 4 CNV lesions per eye). Eyes were enucleated, placed fresh in Tissue-Tek OCT medium (VWR, USA) and stored at -80° C until section preparation and laser microdissection. The day of laser microdissection, eyes were placed on dry ice until cryosection (Cryostat Cryotome FSE, Thermo Scientific). Ten μm sections were performed and place on PEN-Frame slides (Leica, Germany). Regions of interest (ROIs) were microdissected with Leica Laser Microdissection LMD 7000 and directly collected in lysis buffer for subsequent RNA extraction. Samples were collected from 3 different ROIs: control choroid (from control mouse not subjected to CNV), CNV lesion (neovascular tissue from laser-induced mouse) and their corresponding adjacent choroid (healthy tissue next to CNV lesion from laser-induced mouse). For each ROI, microdissected tissues from the two eyes of a single mouse were pooled before RNA extraction.

Intravitreal injections and optical coherence tomography (OCT)

To assess inhibition/overexpression of miR-142-3p, intravitreal injections of inhibitor (single stranded LNA-antimiR) or mimic (chemically modified double-stranded) were performed in mice, just after laser induction (D0, inhibitor conditions), or just after laser induction and 5 days later (D0 + D5, mimic conditions) (n = 11-15 per experimental group for flat-mounted choroids; n = 5-10 per experimental group for flat-mounted retinas). During general anesthesia, mouse eyes were locally anesthetized with Unicaïn 0.4% (Théa Pharma) before the injection, in the vitreous chamber, of a solution (2 μL) of inhibitor (1.83 mM) or mimic (10 μM). Negative control inhibitor and miR-142-3p inhibitor were purchased from Qiagen (miRCURY LNA miRNA Inhibitors, The Netherlands). Mimics (negative control and miR-142-3p mimic) were from Ambion (mirVana miRNA Mimics, USA). LNA-antimiR-142-3p sequence is 5'-AAGTAGGAAACACTAC-3'. After intravitreal injection, eyes were covered with Trafloxal (Bausch + Lomb, Austria) to avoid any infection and inflammation. Both eyes of a single mouse received the same treatment. Phenotypic alterations consequent to miR-142-3p modulation were assessed through optical coherence tomography (OCT) measurements by using the MicronIV instrument, through vascular and microglia stainings on flat-mounted choroids, and through microglia staining on flat-mounted retinas. OCT measurements are presented as (b-c)/c ratios, where b is the CNV lesion thickness and c the adjacent choroid thickness [7]. For miR-142-3p mimic conditions, FITC-dextran (FD2000S, Sigma, USA) tail vein injections were performed 3 minutes before sacrifice.

RNA extraction, reverse transcription and qRT-PCR

Laser-captured choroids or cells were homogenized in lysis buffer by vortexing. For some qRT-PCR, whole retinas and choroids were lysed with ceramic beads (MagNA Lyser Green beads, Roche, Switzerland) in lysis buffer with tissue homogenizer (Precellys Evolution, Bertin, France). RNA was then extracted with miRNeasy Micro kit (laser-captured choroids) (Qiagen) or with mirVana kit (all other experiments) (Ambion), according to the manufacturer's protocols. Complementary DNA was synthesized with miScript RT Kit II (Qiagen) using the same RNA input according to the manufacturer's instructions. mRNA levels of different targets and a set of microRNA levels were quantified by qRT-PCR using FastStart SYBR Green Master (Roche) and a LightCycler 96 instrument (Roche). MiRNA levels were assessed with miRCURY LNA miRNA PCR Assay (Qiagen). All data were normalized to GAPDH and snU6 expression as housekeeping genes. Primer sequences used to detect mouse and human target mRNAs are presented in Table 1. The qRT-PCR results are presented as expression

Table 1. Forward (f) and reverse (r) primer sequences for mouse (mmu) and human (hsa) target mRNAs.

	5' - sequence - 3'
mmu-GAPDH	f: ggtggacctcatggcctaca
	r: ctctcttgctcagtgtccttgct
mmu-uPA	f: taaaatgctgtgtgctgcgg
	r: gcggccttcgatgttacaga
mmu-hsa-snU6	f: cgcttcggcagcacatatac
	r: ttcacgaatttgcgtgtcat
hsa-GAPDH	f: acccactcctccacctttgac
	r: accctgttgctgtagccaaatt
hsa-CD68	f: cagggaatgactgtcctcaca
	r: ctctgtaaccgtgggtgtca
hsa-VEGFa	f: cctccgaaaccatgaacttt
	r: atgattctgccctcctctt

ratios between gene (or microRNA) of interest (GOI) expression and normalizers (NOR) expression. The methodology used for normalization was the following:

$$\frac{2^{-Ctmean\,GOI}}{2^{-Ctmean\,NOR}} = GOI\,expression\,ratio$$

Western blotting

Cells were lysed with 1X lysis buffer (9803, Cell Signaling, USA) containing protease and phosphatase inhibitors (Complete and Phos-STOP, Roche). Proteins (15 μg) were separated on acrylamide gels and transferred onto PVDF membranes. BCLAF1 proteins were detected by overnight incubation, at 4°C, with recombinant anti-BTF antibody (1/10 000 dilution) (Ab181240, Abcam, UK) followed by 1h incubation, at room temperature, with horseradish peroxidase-coupled secondary antibody (7074, Cell signaling) and enhanced chemiluminescent substrate (NEL1040001EA, PerkinElmer, USA) using a LAS4000 imager (Fujifilm). GAPDH (1/10 000, MAB 374, Millipore, USA) was used as a loading control.

Immunohistochemistry

For mouse microglia immunostaining, eyes were enucleated and fixed in paraformaldehyde 4% for 1 hour. Subsequently, retinas and choroids were isolated, permeabilized, blocked and incubated with anti-Iba1 antibody (1/1000 dilution) (Abcam Ab178846) overnight, at room temperature. The next day, samples were washed, incubated with secondary antibody (1/200 dilution) (goat anti-rabbit AlexaFluor 595, Invitrogen

A11012, USA) for 2 hours and washed again. Retinas and choroids were flat-mounted with Fluoromount-G (SouthernBiotech, The Netherlands) on glass-slides for microscopy imaging.

For mouse vascular immunostaining, eyes were enucleated and fixed in ethanol 70 % for 1 hour. Subsequently, choroids were isolated, permeabilized, blocked and incubated with anti-CD31 antibody (1/150 dilution) (Pharmingen 553370) overnight, at room temperature. The next day, samples were washed, incubated with secondary antibody (1/200 dilution) (goat anti-rat AlexaFluor 488, Invitrogen A11006) for 2 hours and washed again. Choroids were flat-mounted with Fluoromount-G (Southern-Biotech) on glass-slides for microscopy imaging.

Epifluorescence/confocal microscopy and image quantifications

Flat-mounted Iba1/CD31 stained choroids were observed under an Olympus Vanox epifluorescence microscope (inhibitors conditions). Flat-mounted Iba1/FITC stained choroids were observed under a Leica Sp5 confocal microscope (mimics conditions) and Z-stacks (z-path = 2.5 μm) were taken. Each CNV lesion was separately imaged and maximum intensity projections were performed for Iba1/FITC images. For each CNV lesion, the area occupied by the staining was calculated with Fiji software [50]. The mean area for a single eye was than calculated for each staining. The percentage of stained area within an eye, normalized to control condition, was used for subsequent statistical analysis to determine vascular and microglia densities.

For cell solidity analysis, Z-stacks of flat-mounted Iba1 stained retinas were taken with a high-resolution confocal microscope (Zeiss LSM 880 with Airyscan), at the 20X magnification. Every CNV lesion was separately imaged, each image representing a 780 μm long square, englobing one CNV area and the surrounding tissue. After acquisition, images were first processed and then quantified. The processing procedure started by identifying image background with morphological opening operations and subtracting it from the raw images. They were then thresholded using Otsu's method and subjected to a median filter to reduce noise. First quantification steps consisted in detecting every objects of the image and discarding the ones which were too small/big to be an isolated cell or a small cell cluster. The bright center of the cells was then used to segment and isolate each cell. Remaining non-cellular objects were discarded using shape and size filters. Finally, tridimensional solidity was measured for every cell. The mean cell solidity of all the CNV lesions area of a single eye was calculated and then used for subsequent data analysis. The solidity of an object is defined as the ratio of the volume of this object over its convex volume. The convex volume corresponds to the volume of the convex hull of the region, i.e. the smallest region that satisfy two conditions: (1) it is convex (2) it contains the original region.

Cell culture

Human microglia HMC3 cells were purchased from ATCC (CRL-3304, USA) and cultured according to the manufacturer's instructions. Cells were seeded in 6-well plate (2.10^5 cells per well) the day before transfection or stimulation. HMC3 were transfected with 5 nM of miR-142-3p inhibitor/negative control inhibitor or with 5 nM miR-142-3p mimic/negative control mimic. Transfection was performed using INTERFERin reagent (Polyplus transfection) following manufacturer's protocol. Cells were harvested 24-hour post-transfection to assess miR-142-3p, BCLAF1 transcript and VEGF-A levels, or 48-hour and 72-hour to assess CD68 and BCLAF1 protein levels, respectively. Alternatively, HMC3 underwent pro-inflammatory stimulation by a 24 hours exposure to 10 ng/mL IFNγ (Recombinant Human IFNγ, Peprotech, USA) or to 0,1 μg/mL LPS (Lipopolysaccharides from *Escherichia coli* 0111:B4, Sigma, USA).

Data analysis

All data and measurements underwent a statistical analysis using Prims7 software. All graphs are presented as mean +/- SEM. Mann-Whitney test or Kruskal-Wallis followed by post-hoc multiple comparisons tests were used to determine statistical significance. Statistical significance was defined as $p \leq 0.05$.

Ethics approval

All *in vivo* experiments were approved by the local Animal Ethic Commission (File number 17-1986, "Commission d'éthique de l'utilisation des animaux de l'Université de Liège").

Availability of data and material

All data generated or analyzed during this study are included in this manuscript and its figures.

Code availability

Custom code for microglia solidity analysis is available on demand.

AUTHOR CONTRIBUTIONS

Q.R. conceptualized the work, performed investigations, interpreted results and wrote the manuscript. J.L. conceptualized the work, performed investigations and reviewed and/or edited the manuscript. T.L., C.Y., L.B. and V.L. performed investigations and reviewed and/or edited the manuscript. V.C. and I.S. reviewed and/or edited the manuscript. A.N. and S.H. conceptualized the work, supervised the study and reviewed and/or edited the manuscript.

CONFLICTS OF INTEREST

The authors declare that they have no conflicts of interest.

REFERENCES

1. WHO. World report on vision. 2019.

2. Flaxman SR, Bourne RR, Resnikoff S, Ackland P, Braithwaite T, Cicinelli MV, Das A, Jonas JB, Keeffe J, Kempen JH, Leasher J, Limburg H, Naidoo K, et al, and Vision Loss Expert Group of the Global Burden of Disease Study. Global causes of blindness and distance vision impairment 1990-2020: a systematic review and meta-analysis. Lancet Glob Health. 2017; 5:e1221–34. https://doi.org/10.1016/S2214-109X(17)30393-5 PMID:29032195

3. Wong WL, Su X, Li X, Cheung CM, Klein R, Cheng CY, Wong TY. Global prevalence of age-related macular degeneration and disease burden projection for 2020 and 2040: a systematic review and meta-analysis. Lancet Glob Health. 2014; 2:e106–16. https://doi.org/10.1016/S2214-109X(13)70145-1 PMID:25104651

4. Adelman RA, Sigler EJ, Seth RK. Age-related Macular Degeneration—Review and Current Concepts. US Ophthalmic Review. 2011; 04. https://doi.org/10.17925/USOR.2011.04.02.119

5. Storey P, Hark L, Haller JA. Age-Related Macular Degeneration. Handbook of Nutrition, Diet and the Eye. 2014. pp. 11–20. https://doi.org/10.1016/B978-0-12-401717-7.00002-2

6. Fletcher EL. Contribution of microglia and monocytes to the development and progression of age related macular degeneration. Ophthalmic Physiol Opt. 2020; 40:128–39. https://doi.org/10.1111/opo.12671 PMID:32017190

7. Lambert V, Lecomte J, Hansen S, Blacher S, Gonzalez ML, Struman I, Sounni NE, Rozet E, de Tullio P, Foidart JM, Rakic JM, Noel A. Laser-induced choroidal neovascularization model to study age-related macular degeneration in mice. Nat Protoc. 2013; 8:2197–211. https://doi.org/10.1038/nprot.2013.135 PMID:24136346

8. Pennesi ME, Neuringer M, Courtney RJ. Animal models of age related macular degeneration. Mol Aspects Med. 2012; 33:487–509. https://doi.org/10.1016/j.mam.2012.06.003 PMID:22705444

9. Park YG, Rhu HW, Kang S, Roh YJ. New Approach of Anti-VEGF Agents for Age-Related Macular Degeneration. J Ophthalmol. 2012; 2012:637316. https://doi.org/10.1155/2012/637316 PMID:22496964

10. Zuber-Laskawiec K, Kubicka-Trzaska A, Karska-Basta I, Pociej-Marciak W, Romanowska-Dixon B. Non-responsiveness and tachyphylaxis to anti-vascular endothelial growth factor treatment in naive patients with exudative age-related macular degeneration. J Physiol Pharmacol. 2019; 70. https://doi.org/10.26402/jpp.2019.5.13 PMID:32009630

11. O'Brien J, Hayder H, Zayed Y, Peng C. Overview of MicroRNA Biogenesis, Mechanisms of Actions, and Circulation. Front Endocrinol (Lausanne). 2018; 9:402. https://doi.org/10.3389/fendo.2018.00402 PMID:30123182

12. Gebert LF, MacRae IJ. Regulation of microRNA function in animals. Nat Rev Mol Cell Biol. 2019; 20:21–37. https://doi.org/10.1038/s41580-018-0045-7 PMID:30108335

13. Bartel DP. Metazoan MicroRNAs. Cell. 2018; 173:20–51. https://doi.org/10.1016/j.cell.2018.03.006 PMID:29570994

14. Xu S, Hazlett LD. MicroRNAs in Ocular Infection. Microorganisms. 2019; 7:359. https://doi.org/10.3390/microorganisms7090359 PMID:31533211

15. Raghunath A, Perumal E. Micro-RNAs and their roles in eye disorders. Ophthalmic Res. 2015; 53:169–86. https://doi.org/10.1159/000371853 PMID:25832915

16. Ménard C, Rezende FA, Miloudi K, Wilson A, Tétreault N, Hardy P, SanGiovanni JP, De Guire V, Sapieha P. MicroRNA signatures in vitreous humour and plasma

of patients with exudative AMD. Oncotarget. 2016; 7:19171–84.
https://doi.org/10.18632/oncotarget.8280
PMID:27015561

17. Kiel C, Berber P, Karlstetter M, Aslanidis A, Strunz T, Langmann T, Grassmann F, Weber BH. A Circulating MicroRNA Profile in a Laser-Induced Mouse Model of Choroidal Neovascularization. Int J Mol Sci. 2020; 21:2689.
https://doi.org/10.3390/ijms21082689
PMID:32294914

18. Liu CH, Huang S, Britton WR, Chen J. MicroRNAs in Vascular Eye Diseases. Int J Mol Sci. 2020; 21:649.
https://doi.org/10.3390/ijms21020649
PMID:31963809

19. Marques-Rocha JL, Samblas M, Milagro FI, Bressan J, Martínez JA, Marti A. Noncoding RNAs, cytokines, and inflammation-related diseases. FASEB J. 2015; 29:3595–611.
https://doi.org/10.1096/fj.14-260323 PMID:26065857

20. Tiwari A, Mukherjee B, Dixit M. MicroRNA Key to Angiogenesis Regulation: MiRNA Biology and Therapy. Curr Cancer Drug Targets. 2018; 18:266–77.
https://doi.org/10.2174/156800961766617063014272
5 PMID:28669338

21. Rakic JM, Lambert V, Munaut C, Bajou K, Peyrollier K, Alvarez-Gonzalez ML, Carmeliet P, Foidart JM, Noël A. Mice without uPA, tPA, or plasminogen genes are resistant to experimental choroidal neovascularization. Invest Ophthalmol Vis Sci. 2003; 44:1732–39.
https://doi.org/10.1167/iovs.02-0809
PMID:12657615

22. Crespo-Garcia S, Reichhart N, Hernandez-Matas C, Zabulis X, Kociok N, Brockmann C, Joussen AM, Strauss O. In vivo analysis of the time and spatial activation pattern of microglia in the retina following laser-induced choroidal neovascularization. Exp Eye Res. 2015; 139:13–21.
https://doi.org/10.1016/j.exer.2015.07.012
PMID:26213305

23. Silverman SM, Wong WT. Microglia in the Retina: Roles in Development, Maturity, and Disease. Annu Rev Vis Sci. 2018; 4:45–77.
https://doi.org/10.1146/annurev-vision-091517-034425 PMID:29852094

24. Bao H, Chen YX, Huang K, Zhuang F, Bao M, Han Y, Chen XH, Shi Q, Yao QP, Qi YX. Platelet-derived microparticles promote endothelial cell proliferation in hypertension via miR-142-3p. FASEB J. 2018; 32:3912–23.
https://doi.org/10.1096/fj.201701073R
PMID:29481306

25. Costa T, Fernandez-Villalba E, Izura V, Lucas-Ochoa AM, Menezes-Filho NJ, Santana RC, de Oliveira MD, Araújo FM, Estrada C, Silva V, Costa SL, Herrero MT. Combined 1-Deoxynojirimycin and Ibuprofen Treatment Decreases Microglial Activation, Phagocytosis and Dopaminergic Degeneration in MPTP-Treated Mice. J Neuroimmune Pharmacol. 2020. [Epub ahead of print].
https://doi.org/10.1007/s11481-020-09925-8
PMID:32564332

26. Stankov A, Belakaposka-Srpanova V, Bitoljanu N, Cakar L, Cakar Z, Rosoklija G. Visualisation of Microglia with the use of Immunohistochemical Double Staining Method for CD-68 and Iba-1 of Cerebral Tissue Samples in Cases of Brain Contusions. Pril (Makedon Akad Nauk Umet Odd Med Nauki). 2015; 36:141–45.
https://doi.org/10.1515/prilozi-2015-0062
PMID:27442380

27. Hernández S, Lloreta J. Manual versus laser micro-dissection in molecular biology. Ultrastruct Pathol. 2006; 30:221–28.
https://doi.org/10.1080/01913120500521018
PMID:16825124

28. Grassmann F, Schoenberger PG, Brandl C, Schick T, Hasler D, Meister G, Fleckenstein M, Lindner M, Helbig H, Fauser S, Weber BH. A circulating microrna profile is associated with late-stage neovascular age-related macular degeneration. PLoS One. 2014; 9:e107461.
https://doi.org/10.1371/journal.pone.0107461
PMID:25203061

29. Zhang L, Liu S, Wang JH, Zou J, Zeng H, Zhao H, Zhang B, He Y, Shi J, Yoshida S, Zhou Y. Differential Expressions of microRNAs and Transfer RNA-derived Small RNAs: Potential Targets of Choroidal Neovascularization. Curr Eye Res. 2019; 44:1226–35.
https://doi.org/10.1080/02713683.2019.1625407
PMID:31136199

30. Du X, Hong L, Sun L, Sang H, Qian A, Li W, Zhuang H, Liang H, Song D, Li C, Wang W, Li X. miR-21 induces endothelial progenitor cells proliferation and angiogenesis via targeting FASLG and is a potential prognostic marker in deep venous thrombosis. J Transl Med. 2019; 17:270.
https://doi.org/10.1186/s12967-019-2015-z
PMID:31416448

31. Fan B, Jin Y, Zhang H, Zhao R, Sun M, Sun M, Yuan X, Wang W, Wang X, Chen Z, Liu W, Yu N, Wang Q, et al. MicroRNA-21 contributes to renal cell carcinoma cell invasiveness and angiogenesis via the PDCD4/c-Jun (AP-1) signalling pathway. Int J Oncol. 2020; 56:178–92.
https://doi.org/10.3892/ijo.2019.4928
PMID:31789394

32. Walz JM, Wecker T, Zhang PP, Cakir B, Gruening B, Agostini H, Reuer T, Ludwig F, Boneva S, Faerber L, Lange C, Schlunck GR, Stahl A. Impact of angiogenic activation and inhibition on miRNA profiles of human retinal endothelial cells. Exp Eye Res. 2019; 181:98–104.
https://doi.org/10.1016/j.exer.2019.01.006
PMID:30615884

33. Romano GL, Platania CB, Drago F, Salomone S, Ragusa M, Barbagallo C, Di Pietro C, Purrello M, Reibaldi M, Avitabile T, Longo A, Bucolo C. Retinal and Circulating miRNAs in Age-Related Macular Degeneration: An *In vivo* Animal and Human Study. Front Pharmacol. 2017; 8:168.
https://doi.org/10.3389/fphar.2017.00168
PMID:28424619

34. Tong N, Jin R, Zhou Z, Wu X. Involvement of microRNA-34a in Age-Related Susceptibility to Oxidative Stress in ARPE-19 Cells by Targeting the Silent Mating Type Information Regulation 2 Homolog 1/p66shc Pathway: Implications for Age-Related Macular Degeneration. Front Aging Neurosci. 2019; 11:137.
https://doi.org/10.3389/fnagi.2019.00137
PMID:31249522

35. Shrestha A, Mukhametshina RT, Taghizadeh S, Vásquez-Pacheco E, Cabrera-Fuentes H, Rizvanov A, Mari B, Carraro G, Bellusci S. MicroRNA-142 is a multifaceted regulator in organogenesis, homeostasis, and disease. Dev Dyn. 2017; 246:285–90.
https://doi.org/10.1002/dvdy.24477 PMID:27884048

36. Mandolesi G, De Vito F, Musella A, Gentile A, Bullitta S, Fresegna D, Sepman H, Di Sanza C, Haji N, Mori F, Buttari F, Perlas E, Ciotti MT, et al. miR-142-3p Is a Key Regulator of IL-1β-Dependent Synaptopathy in Neuroinflammation. J Neurosci. 2017; 37:546–61.
https://doi.org/10.1523/JNEUROSCI.0851-16.2016
PMID:28100738

37. Huang P, Sun J, Wang F, Luo X, Feng J, Gu Q, Liu T, Sun X. MicroRNA Expression Patterns Involved in Amyloid Beta-Induced Retinal Degeneration. Invest Ophthalmol Vis Sci. 2017; 58:1726–35.
https://doi.org/10.1167/iovs.16-20043
PMID:28324113

38. Chaudhuri AD, Yelamanchili SV, Marcondes MC, Fox HS. Up-regulation of microRNA-142 in simian immunodeficiency virus encephalitis leads to repression of sirtuin1. FASEB J. 2013; 27:3720–29.
https://doi.org/10.1096/fj.13-232678 PMID:23752207

39. Carofino BL, Dinshaw KM, Ho PY, Cataisson C, Michalowski AM, Ryscavage A, Alkhas A, Wong NW, Koparde V, Yuspa SH. Head and neck squamous cancer progression is marked by CLIC4 attenuation in tumor epithelium and reciprocal stromal upregulation of miR-142-3p, a novel post-transcriptional regulator of CLIC4. Oncotarget. 2019; 10:7251–75.
https://doi.org/10.18632/oncotarget.27387
PMID:31921386

40. Guiot J, Cambier M, Boeckx A, Henket M, Nivelles O, Gester F, Louis E, Malaise M, Dequiedt F, Louis R, Struman I, Njock MS. Macrophage-derived exosomes attenuate fibrosis in airway epithelial cells through delivery of antifibrotic miR-142-3p. Thorax. 2020; 75:870–81.
https://doi.org/10.1136/thoraxjnl-2019-214077
PMID:32759383

41. Ba J, Peng RS, Xu D, Li YH, Shi H, Wang Q, Yu J. Intravitreal anti-VEGF injections for treating wet age-related macular degeneration: a systematic review and meta-analysis. Drug Des Devel Ther. 2015; 9:5397–405.
https://doi.org/10.2147/DDDT.S86269
PMID:26451092

42. Young K, Morrison H. Quantifying Microglia Morphology from Photomicrographs of Immunohistochemistry Prepared Tissue Using ImageJ. J Vis Exp. 2018; 57648.
https://doi.org/10.3791/57648
PMID:29939190

43. Damani MR, Zhao L, Fontainhas AM, Amaral J, Fariss RN, Wong WT. Age-related alterations in the dynamic behavior of microglia. Aging Cell. 2011; 10:263–76.
https://doi.org/10.1111/j.1474-9726.2010.00660.x
PMID:21108733

44. Zanier ER, Fumagalli S, Perego C, Pischiutta F, De Simoni MG. Shape descriptors of the "never resting" microglia in three different acute brain injury models in mice. Intensive Care Med Exp. 2015; 3:39.
https://doi.org/10.1186/s40635-015-0039-0
PMID:26215806

45. Gupta N, Jadhav S, Tan KL, Saw G, Mallilankaraman KB, Dheen ST. miR-142-3p Regulates BDNF Expression in Activated Rodent Microglia Through Its Target CAMK2A. Front Cell Neurosci. 2020; 14:132.
https://doi.org/10.3389/fncel.2020.00132
PMID:32508597

46. Kwak N, Okamoto N, Wood JM, Campochiaro PA. VEGF is major stimulator in model of choroidal neovascularization. Invest Ophthalmol Vis Sci. 2000; 41:3158–64.
PMID:10967078

47. Huang H, Parlier R, Shen JK, Lutty GA, Vinores SA. VEGF receptor blockade markedly reduces retinal microglia/macrophage infiltration into laser-induced CNV. PLoS One. 2013; 8:e71808.
https://doi.org/10.1371/journal.pone.0071808
PMID:23977149

48. Martínez Leo EE, Segura Campos MR. Neuroprotective effect from Salvia hispanica peptide fractions on pro-inflammatory modulation of HMC3 microglial cells. J Food Biochem. 2020; 44:e13207.
https://doi.org/10.1111/jfbc.13207 PMID:32207175

49. Cappoli N, Mezzogori D, Tabolacci E, Coletta I, Navarra P, Pani G, Dello Russo C. The mTOR kinase inhibitor rapamycin enhances the expression and release of pro-inflammatory cytokine interleukin 6 modulating the activation of human microglial cells. EXCLI J. 2019; 18:779–98.
https://doi.org/10.17179/excli2019-1715
PMID:31645839

50. Schindelin J, Arganda-Carreras I, Frise E, Kaynig V, Longair M, Pietzsch T, Preibisch S, Rueden C, Saalfeld S, Schmid B, Tinevez JY, White DJ, Hartenstein V, et al. Fiji: an open-source platform for biological-image analysis. Nat Methods. 2012; 9:676–82.
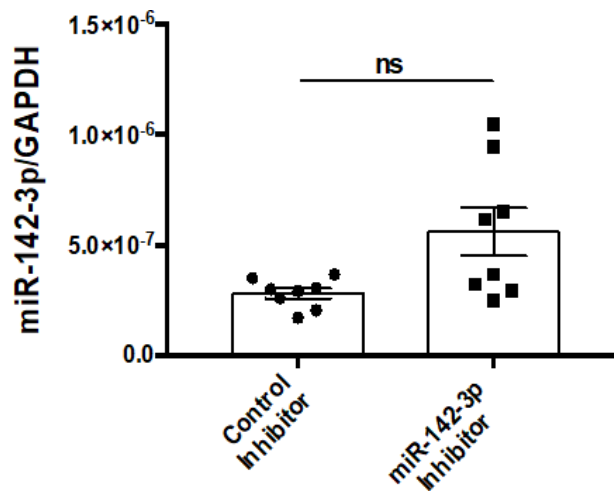https://doi.org/10.1038/nmeth.2019
PMID:22743772

SUPPLEMENTARY MATERIALS

Supplementary Figures
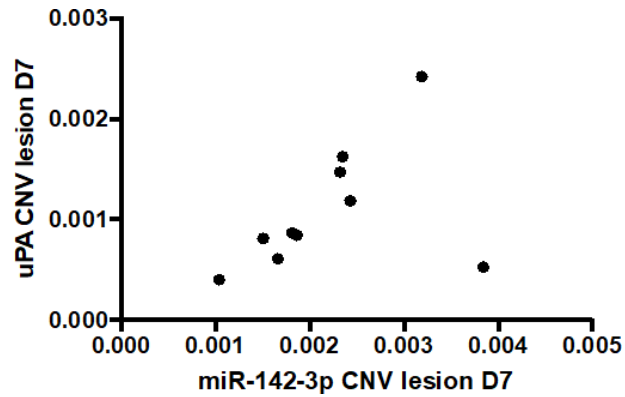
Supplementary Figure 1. Spearman correlation between uPA level and miR-142-3p level in CNV lesion 7 days post laser induction (r = 0.503; p = 0.144).


Supplementary Figure 2. Expression of miR-142-3p was measured in CNV mouse retinas 7 days post laser-induction and intravitreal injection of miR-142-3p inhibitor and relative negative control (n = 8 per experimental group) (ns = not significant).
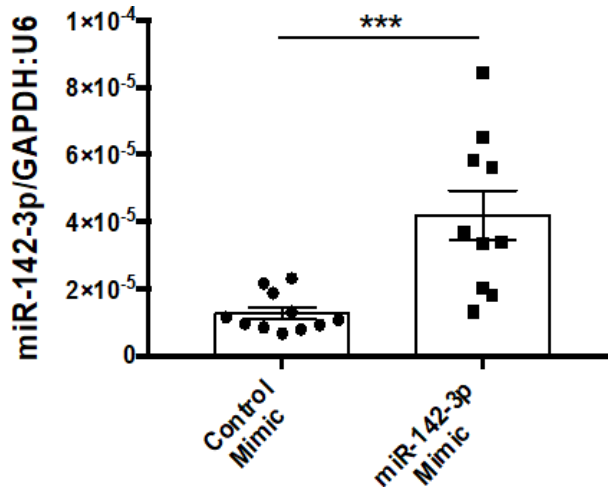
Supplementary Figure 3. Expression of miR-142-3p was measured in CNV mouse retinas 7 days post laser-induction and intravitreal injection of miR-142-3p mimic and relative negative control (n = 10-11 per experimental group) (* = p ≤ 0.001).**
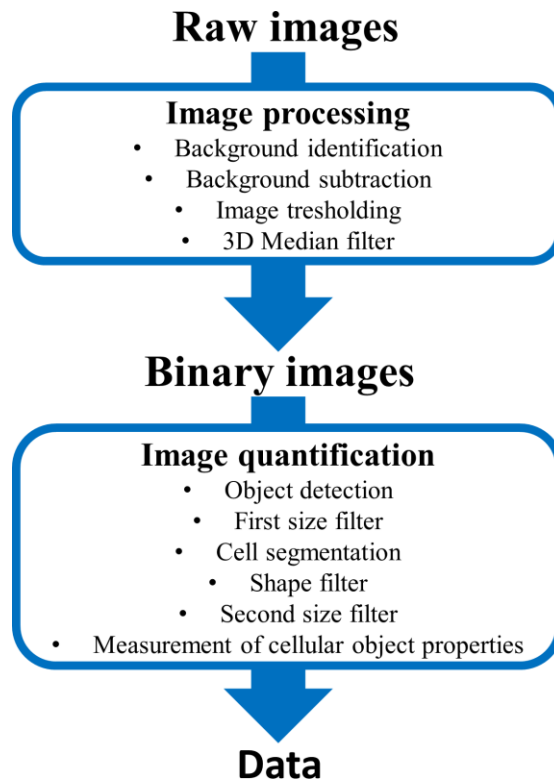
Supplementary Figure 4. Workflow chart of image processing and quantification for microglia solidity analysis in flat-mounted retinas.
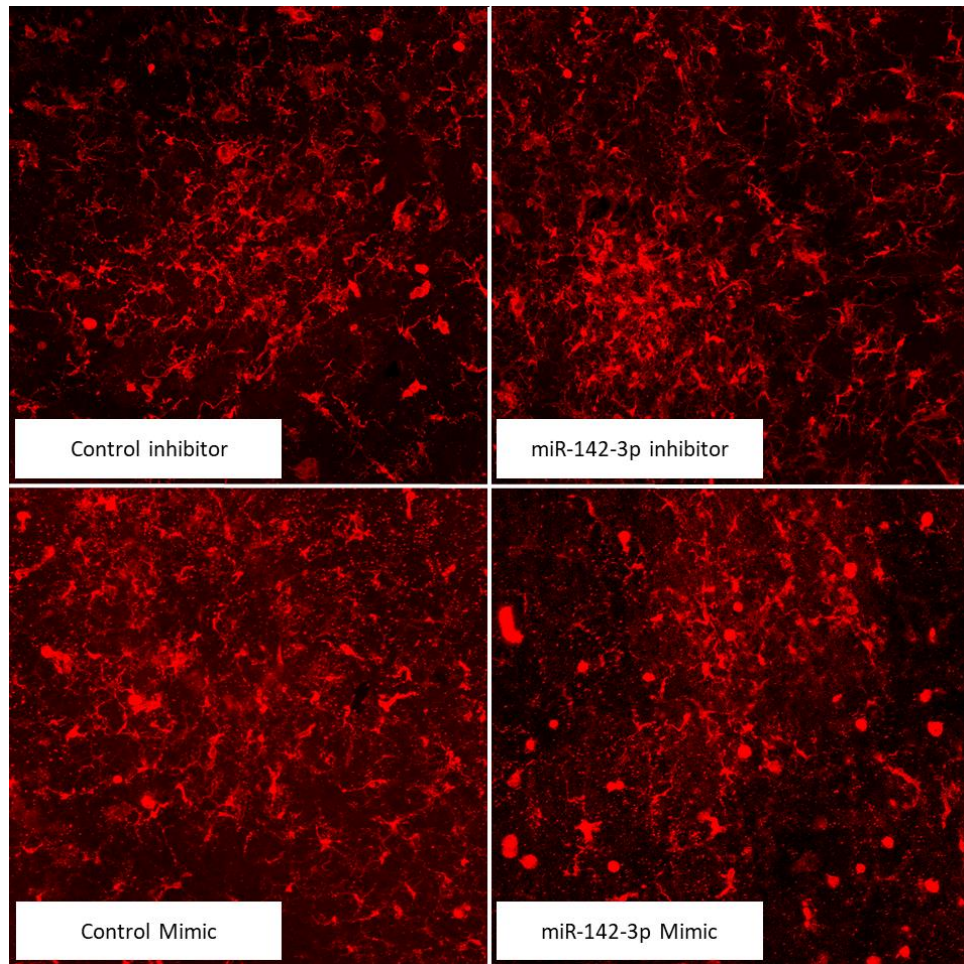
Supplementary Figure 5. Representative raw images of Iba-1 stained flat-mounted retinas for miR-142-3p and relative control inhibitors (top panels) and miR-142-3p and relative control mimics (bottom panels) treatment.